









Synthesis and characterization of mechanically strong carboxymethyl cellulose–gelatin–hydroxyapatite nanocomposite for load-bearing orthopedic application

Chandrani Sarkar^{1,2} , Pushpa Kumari¹ , Kumar Anuvrat³ , Sumant Kumar Sahu² ,
Jui Chakraborty⁴ , and Subhadra Garai^{1,*} 

¹Advance Material and Processing Division, CSIR-National Metallurgical Laboratory, Jamshedpur 831007, India

²Department of Applied Chemistry, Indian Institute of Technology (ISM), Dhanbad, Jharkhand 826004, India

³Centre for Nanotechnology, Central University of Jharkhand, Ranchi 835205, India

⁴CSIR-Central Glass and Ceramic Research Institute, 196, Raja S.C. Mullick Road, Jadavpur, 700 032 Kolkata, India

Received: 1 June 2017

Accepted: 29 August 2017

Published online:

5 September 2017

© Springer Science+Business
Media, LLC 2017

ABSTRACT

Novel three-dimensional hybrid polymer–hydroxyapatite nanocomposites have been developed as load-bearing synthetic bone graft through in situ mineralization process, using natural polymers carboxymethyl cellulose (CMC) and gelatin (Gel) as matrix. This process is simple and does not involve any chemical cross-linker. Detailed structural and physicochemical characterization of the samples disclosed that incorporation of gelatin with CMC assists the formation of CMC-Gel polymeric network of new conformational structure through non-covalent interactions (H-bond). The formation of hydroxyapatite (HA) in this polymeric network was occurred in such a fashion that the HA serves as bridging molecule which strengthen the polymeric network more and formed a mechanically strong three-dimensional CMC-Gel-HA nanocomposite. The synthesized CMC-Gel-HA nanocomposites have compressive strength and modulus in the range of 40–86 MPa and 0.4–1.2 GPa, respectively, analogous to human cancellous as well as cortical bone. In vitro cell interaction of the synthesized nanocomposites with osteoblast-like MG-63 cells has been evaluated. Results showed that synthesized CMC-Gel-HA nanocomposite promote cells for high alkaline phosphatase activity and extracellular mineralization. Extracellular mineralization ability of nanocomposite was investigated by alizarin red staining and von Kossa staining. Biodegradable nature and bone apatite formation ability of CMC-Gel-HA nanocomposite under simulated physiological environment were investigated by different characterization processes. Results indicated that the synthesized CMC-Gel-HA nanocomposite has great potential to be used as regenerative bone graft in major load-bearing region.

Address correspondence to E-mail: subha@nmlindia.org

Introduction

Nowadays, the treatment of diseased and damaged bone by the suitable bone substitute is a great challenge for clinicians. It needs to replace defected tissues with a viable functioning alternative substitute [1]. Globally, an autograft is considered as the gold standard for bone regeneration/bone defect repairing. But due to its limitation of accessibility and risk of donor site morbidity, an alternative strategy for bone grafting is required in the form of synthetic bone grafts that can augment bone regeneration [2–6]. Therefore, researchers focused on the development of polymer–hydroxyapatite nanocomposites as bone graft materials/scaffolds [7–9]. In most of the articles, *in situ* mineralization process is adopted for the synthesis of polymer–hydroxyapatite nanocomposites. It is a bioinspired process in which mineralization occurs in polymer matrix, similar to the biomineralization of hydroxyapatite (HA) in association with extracellular matrix (ECM) of natural bone [10, 11]. However, the poor mechanical strength of polymer–HA composite restricts its application as non-load-bearing powder material. To circumvent this problem, extensive research is focused to match the structure–mechanical properties of polymer–HA composites with natural bone [12–15].

Natural bone is an anisotropic complex of collagen (COL) and hydroxyapatite. From last decades, researchers have developed collagen–HA nanocomposites in order to mimic the structure and composition of natural bone [16–18]. But the application of type-1 COL in bone tissue engineering field is limited due to its high price and poor availability. Hence, gelatin has been recognized as an alternative option by many researchers [19–23]. Gelatin is a denatured form of collagen having Arg-Gly-Asp (RGD) sequence and exhibits good biocompatibility, low immunogenicity and low cost. Further, the association of gelatin with polysaccharides forms a complex similar to extracellular matrix (ECM) and facilitates the attachment, growth and proliferation of human osteoblasts cells, making it most suitable complex for tissue engineering [24–27]. Generally, this type of association in polysaccharides and gelatin was fabricated by using chemical cross-linker which may cause safety problems in body.

Among other polysaccharides, cellulose is an abundant and cheapest viscous polymer, widely used

in the fabrication of orthopedic biomaterial/scaffolds [28–30]. Moreover, the combination of cellulose and gelatin has been utilized by many researchers to develop mechanically and thermally stable cellulose–gelatin complex/film based on non-covalent interaction [31–33]. The cellulose–gelatin complex is being potentially used in drug delivery and tissue engineering [34, 35]. Several studies have shown that the incorporation of hydroxyapatite with polysaccharides–gelatin complex provides good mechanical strength to scaffolds due to excellent mechanical properties of nanosized hydroxyapatite [36–39]. Furthermore, the presence of polysaccharides such as chitosan [40] and alginates [41] induce the orderly deposition of HA crystals in gelatin–polysaccharide system with controlled morphology as same as in natural bone.

In our previous report, we have synthesized biomimetic carboxymethyl cellulose–HA nanocomposite for load-bearing application [42]. In this study, we have aimed to develop self-assembled hybrid polymers–HA nanocomposite with enhanced mechanical strength and bioactivity by mimicking phenomenal science of nature. In nature, sophisticated functional materials are developed through hierarchical self-assembly of molecules into structurally stable arrangements by the driving force of non-covalent interactions, including hydrogen bonds, ionic bonds and electrostatic interaction [43–45]. Pei et al. [46] demonstrated an efficient strategy to fabricate cellulose/gelatin sponge for wound dressing based on intermolecular H-bonding between cellulose and gelatin. Therefore, we blended gelatin with carboxymethyl cellulose to form a self-assembled CMC-Gel matrix. The present study also demonstrated the *in situ* mineralization of hydroxyapatite on stable CMC-Gel matrix by electrostatic interaction and formed a mechanically strong three-dimensional CMC-Gel-HA nanocomposite. The structural and mechanical properties of synthesized nanocomposites were thoroughly characterized. *In vitro* biocompatibility, cell attachment and cell differentiation study with osteoblast-like MG-63 cell were carried out on the ternary nanocomposites. We have also studied the *in vitro* assessment of apatite formation and degradation under simulated physiological conditions. The synthesized CMC-Gel-HA nanocomposite has few advantageous properties compared with other reported hybrid polymer–HA

nanocomposites [36–38, 47–52]: (a) three-dimensional nanocomposite has been developed by self-assembly of CMC, gelatin and HA, without using any cross-linker; (b) synthesized nanocomposite has high mechanical strength being in the range of human cancellous as well as cortical bone; and (c) CMC-Gel-HA nanocomposite promotes proliferation and differentiation of MG-63 cells.

Experimental procedures

Materials

All the chemicals like analytical grade diammonium hydrogen phosphate $[(\text{NH}_4)_2\text{HPO}_4]$, calcium nitrate tetra-hydrate $[\text{Ca}(\text{NO}_3)_2 \cdot 4\text{H}_2\text{O}]$ (with $\geq 98\%$ assay), liquid ammonia (with $>25\%$ assay), gelatin (pH 3.8–7.6) and sodium salt of carboxymethyl cellulose (CMC) (degree of substitution 0.9) were procured from Merck, Mumbai, India. Deionized (DI) water was used in all the experiment.

Synthesis of three-dimensional CMC-Gel-HA nanocomposites

In this study, CMC-Gel-HA nanocomposites were synthesized in three different compositions with the variation of CMC and gelatin content (Table 1). These nanocomposites were labeled as HA-5, HA-10 and HA-15, respectively. For the synthesis of each composite, desired amount of CMC was dissolved in different vessels containing 1200 mL of DI water with gentle heating and continuous stirring by using magnetic stirrer for 5 h. Subsequently, desired amount of gelatin was also dissolved in different vessels containing 500 mL of DI water and stirred for 1 h at room temperature. Then, it is slowly added to CMC solution and stirred well for half an hour. One hundred and eighteen grams of calcium nitrate tetrahydrate was dissolved in 500 mL of deionized water (DI). The prepared calcium nitrate (0.99 M) solution

was slowly added to polymer solution with continuous stirring. The pH was maintained at 10–11 by adding aqueous ammonia solution and kept for 24 h of aging at 30 °C. Thirty-seven grams of diammonium hydrogen phosphate was dissolved in 500 mL DI water and made alkaline with ammonia solution. The prepared diammonium hydrogen phosphate (0.56 M) solution was slowly added to calcium–polymer solution. Milky white coloration was observed instantaneously, and the total volume of the slurry was made up to 3500 mL by adding DI water, allowed to age for a week at 30 °C. After aging, the slurry was washed with DI water to neutralize. Neutralized slurry was transferred to Teflon beaker and dried in an oven at 50 °C for 72 h to obtain the three-dimensional nanocomposite (50 g). For comparative study, three-dimensional CMC-HA nanocomposite was also prepared and labeled as HA-0 [42].

Characterization

The infrared (IR) spectra of CMC, Gel and nanocomposites were acquired by using Fourier transform infrared (FTIR) [JASCO-FTIR, Model 410] spectrometer. IR spectrum of the mixture of polymers was also taken to observe the effect of hybridization. Gelatin and CMC were dissolved in DI water, kept for 24 h and then dried. Solid-state carbon-13 nuclear magnetic resonance (^{13}C -NMR) measurement of CMC, Gel, CMC-HA and CMC-Gel-HA nanocomposite was carried out by using ECX400-Jeol 400 MHz high-resolution multinuclear Fourier transform nuclear magnetic resonance (FT-NMR) spectrometer. The mineral phase and its crystallite size in synthesized nanocomposites were identified by using X-ray diffractometer (XRD) (Bruker, D₈ Discover CuK α radiation with $\lambda = 0.154$ nm, 40 kV, 40 mA). For each nanocomposite, data were collected over the 2θ range 20–80° with a scan speed 0.4 s per step. For microstructural analysis, the synthesized nanocomposites were crushed and powdered. These powder samples were dispersed in ethanol by ultra-probe sonication for 20 min and dropped on carbon-coated Cu-grid. After drying the grids under IR lamp, the microstructural features of nanocomposites were captured by using transmission electron microscopy (TEM cm200, CX Philips JEOL 2100) at an accelerating voltage of 120 kV. Thermogravimetric analysis (TGA) was carried out in thermogravimetric

Table 1 Weight (%) of CMC and gelatin

Samples	CMC (wt%)	Gelatin (wt%)
HA-0	30	0
HA-5	25	5
HA-10	20	10
HA-15	15	15

analyzer (Netzsch STA 449 C), over 25–1200 °C temperature range at a heating rate of 10 °C min⁻¹. The surface morphology of the as-synthesized nanocomposites was observed by field-emission scanning electron microscope (FESEM Leo s4302 UK) for which samples were coated with silver. The porosity percentage of nanocomposites was determined by conventional liquid displacement method [38, 42]. The ethanol was used as a displacing liquid because it penetrates the pores easily. The pore size distribution in each composite was determined by mercury intrusion porosimetry (Model PASCAL 140/440). The compressive strength and elastic modulus of the nanocomposite of dimension (16 mm × 8 mm × 8 mm) were determined using a universal testing machine (UTM, QMAT 3.75, and ASTM D695). To check the reproducibility, at least three specimens were tested for each nanocomposite.

In vitro biocompatibility and cell adhesion studies

Osteoblast-like MG-63 cells were used for in vitro cell study. MG-63 cells were derived from osteosarcoma, though they retained important osteogenic cell differentiation markers, such as the activity of alkaline phosphatase and osteocalcin production; thus, these cells are considered as good in vitro model for testing the interaction of materials with bone cells [53, 54]. Here, cells were grown to subconfluency in Dulbecco's modified Eagle medium (DMEM) supplemented with 10% fetal bovine serum (FBS), 2 mg mL⁻¹ NaHCO₃, 1 µg mL⁻¹ penicillin G, 1 mg mL⁻¹ streptomycin, in a humidified incubator at 37 °C with 5% CO₂ (HF90 Heal Force, China). 3-[4,5-Dimethylthiazol-2-yl]-2,5-diphenyltetrazolium bromide (MTT) assay of the samples were performed by indirect method as per the guidelines of ISO 10993-5. The small pieces of nanocomposites of dimension 2 mm × 2 mm × 0.2 mm were steam sterilized for 20 min, incubated in 1 mL of DMEM for 24 h in humidified incubator at 37 °C with 5% CO₂ and filtered with 0.22-µm membrane filter. Extracts were added on pre-seeded (6 × 10⁴ cells per well) cells in 6-well plates and kept under humidified incubator at 37 °C with 5% CO₂ for 1, 4 and 7 days. Media and samples extract of well plate were replenished with fresh ones on every second day. After incubation for specified period, MTT

[0.2 mg mL⁻¹ in DMEM containing 10% phosphate buffer solution (PBS)] solution was added into each well and incubated in 5% CO₂ incubator at 37 °C for 3 h. Then, MTT solution was removed and dimethyl sulphoxide (DMSO) was added to dissolve the formazan crystals. Colored solution was transferred to 96-well plate, and the absorbance of developed color was recorded at 595 nm by using ELISA plate reader (i-Mark, Bio-Rad, USA).

For cell adhesion study, sterilized nanocomposites of size 2 mm × 2 mm × 0.2 mm were placed in 6-well plate. After that, MG-63 cell suspension at a density of 6 × 10⁴ cells mL⁻¹ was dropped onto the samples of well plate and incubated for 1, 4 and 7 days, respectively. Before proceeding to fixation procedure, images of cells in the presence of nanocomposites were captured by using inverted phase contrast microscope (MOTIC AE31). Then, samples were rinsed three times with PBS and fixed with 4% paraformaldehyde for 10 min. The fixative was removed, and samples were washed with PBS and dehydrated with series of graded ethanol (30, 50, 75, 90, 95 and 100%). The morphological characteristic of adhered cells on the surface of nanocomposites was observed using scanning electron microscope (SEM).

In vitro study of cell differentiation

Osteoblast-like MG-63 cells at a density of 6 × 10⁴ cells per well were seeded into 6-well plate. After 24 h, the sterilized nanocomposites of size 2 mm × 2 mm × 0.2 mm were carefully placed over the cells and maintained in standard culture condition (DMEM) for 7 and 14 days according to published method [23, 55]. Cells cultured in osteogenic media (DMEM with osteogenic supplements) and normal media (DMEM) were set as positive and negative control, respectively. At the end of desired period, alkaline phosphatase (ALP) activity of MG-63 cells was estimated by using alkaline phosphatase activity estimation kit of HiMedia (Product Code—CCK035) according to manufacturer's instruction. The rate of increased absorbance was measured at 405 nm for determining the ALP activity of cell. Finally, ALP activity was normalized with total protein content of cell lysates which was determined by using protein assay kit of HiMedia (Bradford assay, Product Code—HTBC005). Results were representative of three different experiments.

Extracellular mineralization ability of samples was investigated by alizarin red staining and von Kossa staining. As stated above, 6×10^4 cells per well were seeded in 6-well plate and similar culture condition was maintained for 7, 14 and 21 days. After culturing for desired period, samples were removed from well plate. After that, cells of the well plate were fixed with 4% paraformaldehyde for 15 min and washed with biological water. Finally, 1 mL of 2% alizarin solution was added into each well and incubated for 30 min. Excess dye was removed by washing with biological water. Red-stained images of mineralized nodules were captured by using inverted phase contrast microscope (MOTIC AE31). For von Kossa staining, same procedure was followed except 1 mL of 1% silver nitrate solution was added into each well after cell fixation with 4% paraformaldehyde and kept under UV light for 30 min. Residual silver nitrate was removed by washing with biological water. Brownish-blackish images of mineralized nodules were captured by using inverted phase contrast microscope (MOTIC AE31).

In vitro study in simulated body fluid (SBF)

The assessment of apatite formation and biodegradability of samples was evaluated by SBF treatment [9, 50, 55]. SBF was prepared by using graded NaCl, NaHCO₃, KCl, K₂HPO₄·3H₂O, MgCl₂·6H₂O, CaCl₂·2H₂O, Na₂SO₄, Tris (hydroxyl methyl) methyl amine, 1 M HCl proposed by Kokubo [56]. Prepared SBF had ion concentrations (Na⁺ 142.0, K⁺ 5.0, Mg²⁺ 1.5, Ca²⁺ 2.5, Cl⁻ 147.8, HCO₃⁻ 4.2, HPO₄²⁻ 1.0, SO₄²⁻ 0.5 mM) and pH (7.4) nearly equal to human body fluid. Samples of dimension 16 mm × 8 mm × 8 mm were immersed in 30 ml SBF at 37 °C for a maximum period of 1 month. Samples were periodically (1, 2, 3, 4 weeks) withdrawn from SBF solution, rinsed gently with DI water and soaked in blotting paper for removing excess water. Biodegradability of samples was evaluated from weight loss (%) calculated by following formula, weight loss (%) = [(W₀ - W_t)/W₀] × 100, where W₀ is the weight of sample before SBF treatment, while W_t is the weight of sample after SBF treatment at time (t). FTIR spectra of SBF-dipped samples were also acquired after incubation for desired period (7, 14, 21 and 28 days). Apatite deposition on the surface of nanocomposites after immersion in SBF was confirmed by FESEM.

Statistical analysis

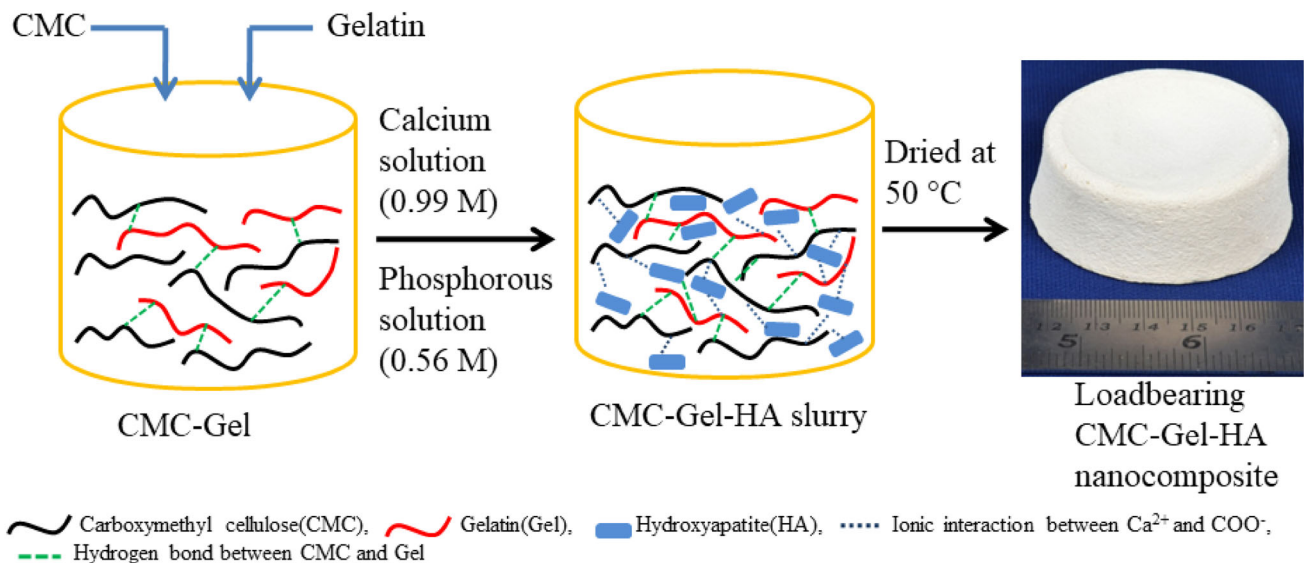
Each experiment was carried out in triplicate, and measured data were expressed as mean ± standard deviation. The data were statistically analyzed by using GraphPad Prism with one-way ANOVA; the value of $p < 0.05$ is considered statistically significant (Scheme 1).

Results and discussion

FTIR and ¹³C-NMR analysis

The formation of three-dimensional CMC-Gel-HA nanocomposite with the effective association of CMC, Gel and HA was established by FTIR analysis. The characteristics FTIR spectra of CMC, Gel and CMC-Gel mixture are shown in Fig. 1a. In CMC-Gel spectrum, we found that the OH⁻ band of CMC and NH⁻ of Gel were overlapped and appeared at 3430 cm⁻¹ due to H-bonding between CMC and gelatin [31, 32, 46]. Noticeably, the COO⁻ (sym. str.) band at 1429 cm⁻¹ of CMC in the presence of gelatin was shifted toward lower wave number at 1384 cm⁻¹ confirming the association of CMC with gelatin through intermolecular H-bonding [46]. Due to these H-bonding, gelatin and CMC macromolecules form a stable polymer network of new conformational structure for in situ mineralization of HA.

According to biomineralization process, early mineralization of HA was initiated at the anionic sites of polymer by electrostatic interaction between Ca²⁺ ions and COO⁻ groups, depicted by many researchers [42, 50–52]. Then, phosphate ions react with calcium ions to form HA molecule, depending on the pH (10–11) of the reaction mixture. In the spectra of nanocomposites (Fig. 1b), we found that the characteristics phosphate bands of HA at 1034, 603 and 564 cm⁻¹ correspond to P–OH, O–P–O and P–O–P vibrations, respectively, confirming the formation of HA in hybrid polymers matrix [40, 57]. In the composite formation stage, the pH of the reaction mixture is higher than the isoelectric point of gelatin where COOH groups of gelatin exist as COO⁻ ions and electrostatically bind with Ca²⁺ ions of HA [40, 58]. In Fig. 1b, we observed that the band which corresponds to COO⁻ group of polymers was shifted at 1639 cm⁻¹, suggesting electrostatic interaction between Ca²⁺ ions of HA and COO⁻ groups of



Scheme 1 Schematic presentation of synthetic procedure of mechanically strong three-dimensional CMC-Gel-HA nanocomposite.

CMC/gelatin. Such interactions might be considered as an evidence for involvement of Ca^{2+} in the formation of bridging structure with CMC and gelatin [52, 59]. The band at 1384 cm^{-1} of CMC-Gel matrix was not shifted in the spectra of CMC-Gel-HA nanocomposites, indicating that the formation of HA at bridging position did not affect the intermolecular linking of CMC-Gel matrix rather strengthened the polymeric network. Evidently, the sharpness of this band increases with gelatin concentration. It may be due to involvement of more $-\text{NH}$ groups (amide II and amide III) in cross-linking [60] that can be further confirmed with the observance of an additional band at $3200\text{--}3160\text{ cm}^{-1}$, indicating the enhanced intermolecular H-bonding with the participation of more number of $-\text{NH}$ group of gelatin [60]. These results confirmed that the interaction/cross-linking among CMC, gelatin and HA in HA-15, HA-10 composite is stronger than HA-0, HA-5.

The solid-state ^{13}C -NMR of CMC, gelatin, CMC-HA and CMC-Gel-HA nanocomposites is shown in Fig. S1. In CMC pattern, the significant peaks at 182, 108, 86, 78 and 65 ppm correspond to COO^- , C1, C2, C3 and C6 of CMC [42, 46]. The peaks of gelatin at 172.80, 69.80, 58.63, 41.85, 28.77 and 24.38 ppm were assigned to COO^- , Hyp γ , Pro- α , Gly α , Pro- β and Pro- γ , in accordance with earlier report [46]. Comparing the spectra of HA-15 with polymers and HA-0, it can be observed that the peaks of CMC and gelatin appeared in the spectrum of HA-15 with downfield shifts confirming the presence of CMC and

gelatin in HA-15 with change of chemical environment. This change attributed to the interactions between polymers and HA nanoparticles. One interesting observation is that peaks of all carbon atoms in HA-15 shifted downfield more than that in HA-0. These results confirm the strong molecular interactions occurred among CMC, gelatin and HA in HA-15 nanocomposite.

XRD and TEM analysis

XRD patterns of synthesized four nanocomposites are shown in Fig. 2a. All the patterns showed characteristics peaks of hydroxyapatite indexed as (002), (102), (211), (202), (310), (222), (004), (213), (511) as JCPDS file (Card No.—09-0432). The crystallite size D (nm) of HA was calculated from the most prominent peak in XRD by following Debye–Scherer formula $D = K \lambda / \beta_{1/2} \cos \theta$, where K is Scherer constant (0.9), λ wavelength (in angstrom) and θ diffraction angle [61]. $\beta_{1/2}$ is the full width of the diffraction peak at half the maximum intensity. It is observed that the crystallite size of nanocomposites (inset Fig. 2a) decreases from 30 to 10 nm with gelatin content, which is of the order of crystallite size found in natural bone [62]. There may be two factors responsible for modulating the crystallite size of HA in CMC-Gel-HA nanocomposites: (1) the intermolecular interaction of organic molecules with the surface of hydroxyapatite suppresses the crystal growth [63] and (2) the space/gap available for growth of bridged

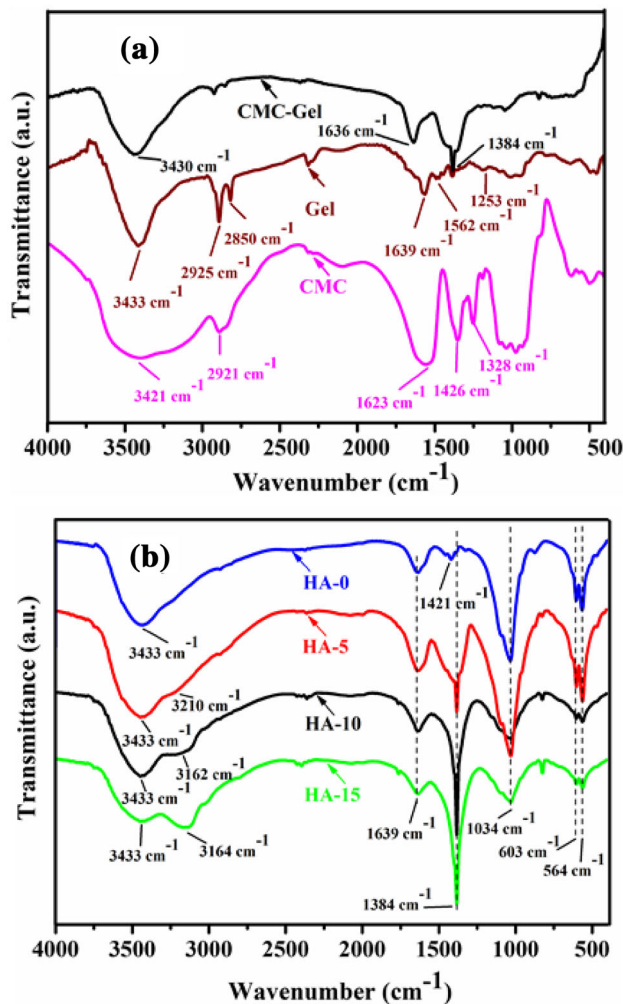


Figure 1 a FTIR spectra of CMC, Gel and CMC-Gel mixture. b FTIR spectra of four synthesized nanocomposites.

HA crystal is reduced due to enhanced cross-linking between CMC and gelatin in CMC-Gel-HA nanocomposite [40].

Bright-field TEM images of CMC-HA nanocomposite [HA-0] and CMC-Gel-HA nanocomposite [HA-15] are shown in Fig. 2b, c. In the image of CMC-HA nanocomposite, we found that the particles are ~30 nm in size with globular shape, whereas the HA particles in CMC-Gel-HA nanocomposite (Fig. 2c) are smaller in size (<20 nm) with elongated morphology. The selected area electron diffraction (SAED) pattern of CMC-Gel-HA nanocomposite (Fig. 2d) shows slightly crescent-shaped diffraction ascribed to (002) plane of HA which indicates that the distribution of HA particles in the composite is slightly oriented with respect to that plane [19],

similar to natural bone where HA crystals grow in parallel with the collagenous fibers along the (002) c-axis [62]. Moreover, the diffused rings of (004), (211) and (002) planes of HA were found in SAED pattern, among which the brightest one represents (211) plane which is consistent with XRD spectra. These results emphasized the role of self-assembled CMC-Gel matrix on the morphology of HA crystals as well as its oriental arrangement. In FTIR, we have already illustrated the formation of new conformational CMC-Gel matrix through H-bonding. We also assumed that the nucleation of HA has been occurred in the bridging position of CMC and gelatin. Initially, the coordination of Ca²⁺ ion with polymeric network stabled the stereochemical arrangement more and HA is grown into the space provided by this arrangement. So, the stereochemical geometry in CMC-gelatin-Ca complexes is supposed to control the mineralization process. The hydroxyapatites mineralized at these sites gradually grow along the extended direction of these macromolecules to the critical size of nucleation and eventually to form an elongated HA particles [41] where HA crystals are formed with the development of preferred orientation [(002) plane]. These results revealed that the assembled CMC-gelatin matrix modulates the morphology of HA particles from globular (in CMC-HA) to needlelike in CMC-Gel-HA nanocomposite and also controlled the size.

Thermogravimetric analysis

The TGA thermograms of synthesized nanocomposites are presented in Fig. S2. There are three stages of weight loss in the nanocomposites: First stage is in the temperature range of 50–200 °C assigned the loss of adsorbed water molecule. The second stage at about 200–600 °C corresponds to the thermal decomposition of the polymeric CMC-Gel matrix [31], and the third stage (600–1000 °C) attributes the dehydroxylation of HA [64]. The weight loss due to decomposition of organic components (CMC and Gel) in HA-0, HA-5, HA-10 and HA-15 was 26, 27, 27 and 29%, respectively, which is slightly less than the actual materials taken in synthesis process that indicates the loss of unbound polymers during washing step. The remaining mass in HA-0, HA-5, HA-10 and HA-15 was 62, 62, 60 and 58%, respectively, which represents the thermally stable HA content.

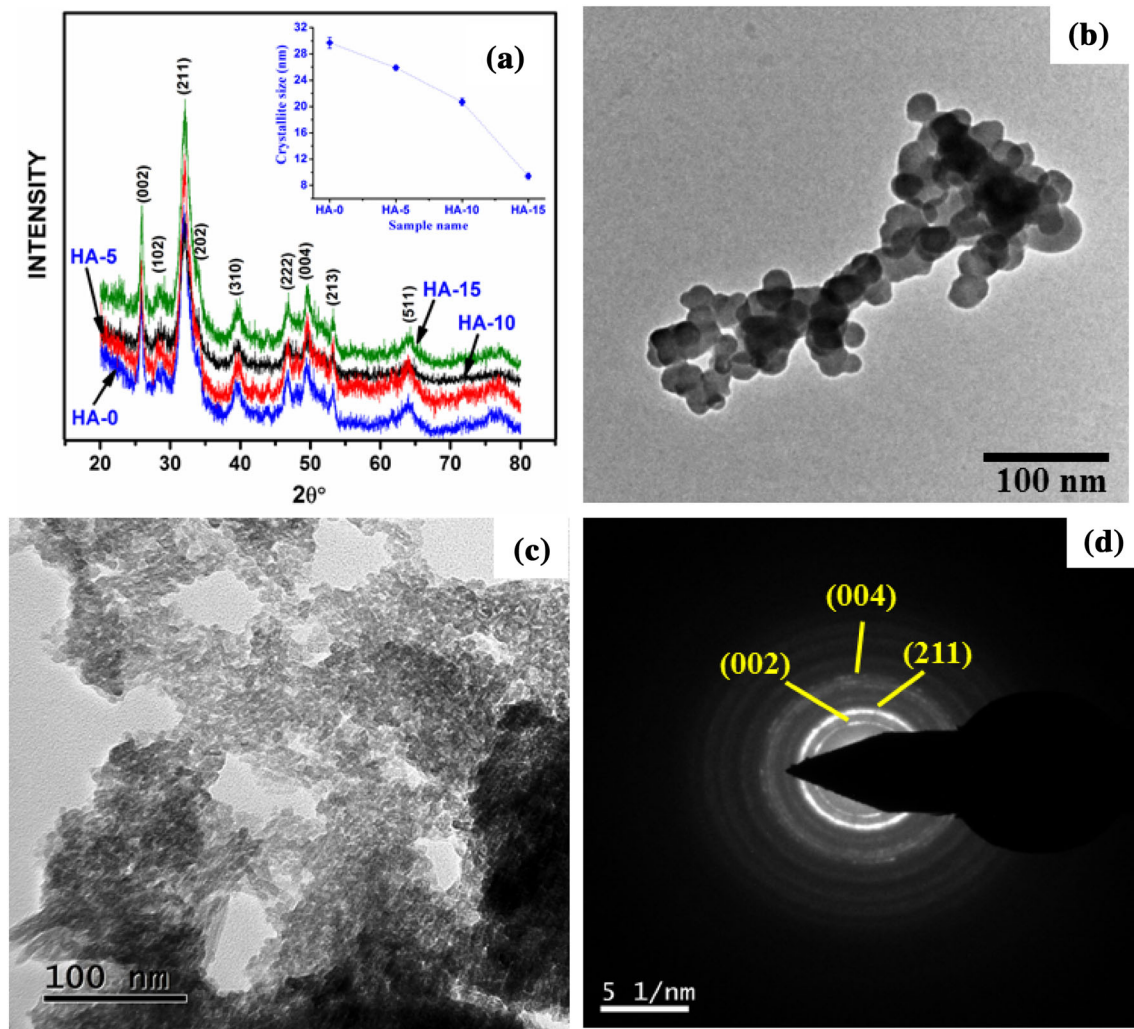


Figure 2 a XRD of as-synthesized nanocomposites [plot of crystallite size is in *inset*]. b TEM image of CMC-HA nanocomposite. c TEM image of CMC-Gel-HA nanocomposite. d SEAD pattern of CMC-Gel-HA nanocomposite.

Surface morphology of synthesized nanocomposites

The microstructure of all the four nanocomposites is shown in Fig. 3. It is observed that the HA nanoparticles aggregated with the formation of a bead-like structure and embedded in a polymeric template. Bead-like morphology is orderly knitted over polymeric network with uniform distribution of irregular shaped interconnected pores. From these FESEM micrographs, we noticed that the size of agglomerates was increased with gelatin content with the formation of a nearly compact structure in HA-15. It indicates that the molecular interaction causes the accretion of nanoparticles and organized them in

such a way that the optimal packing efficiency was achieved in the composites [65].

Pore size distribution of nanocomposites inset in their corresponding FESEM images (Fig. 3). HA-0, HA-5, HA-10 and HA-15 nanocomposites exhibited bimodal distribution of pore size in the broad range of 0.01–100 μm with a corresponding total porosity ~55, 47, 36 and 15%, respectively. However, CMC-Gel-HA nanocomposites (HA-5, HA-10 and HA-15) possess major pores in the range of 0.01–0.1 μm , while in CMC-HA nanocomposite (HA-0) pores in the range of 0.01–100 μm . Result showed that the overall porosity (%) and pore volume for macropores was decreased with gelatin content which is in good agreement with corresponding FESEM images of

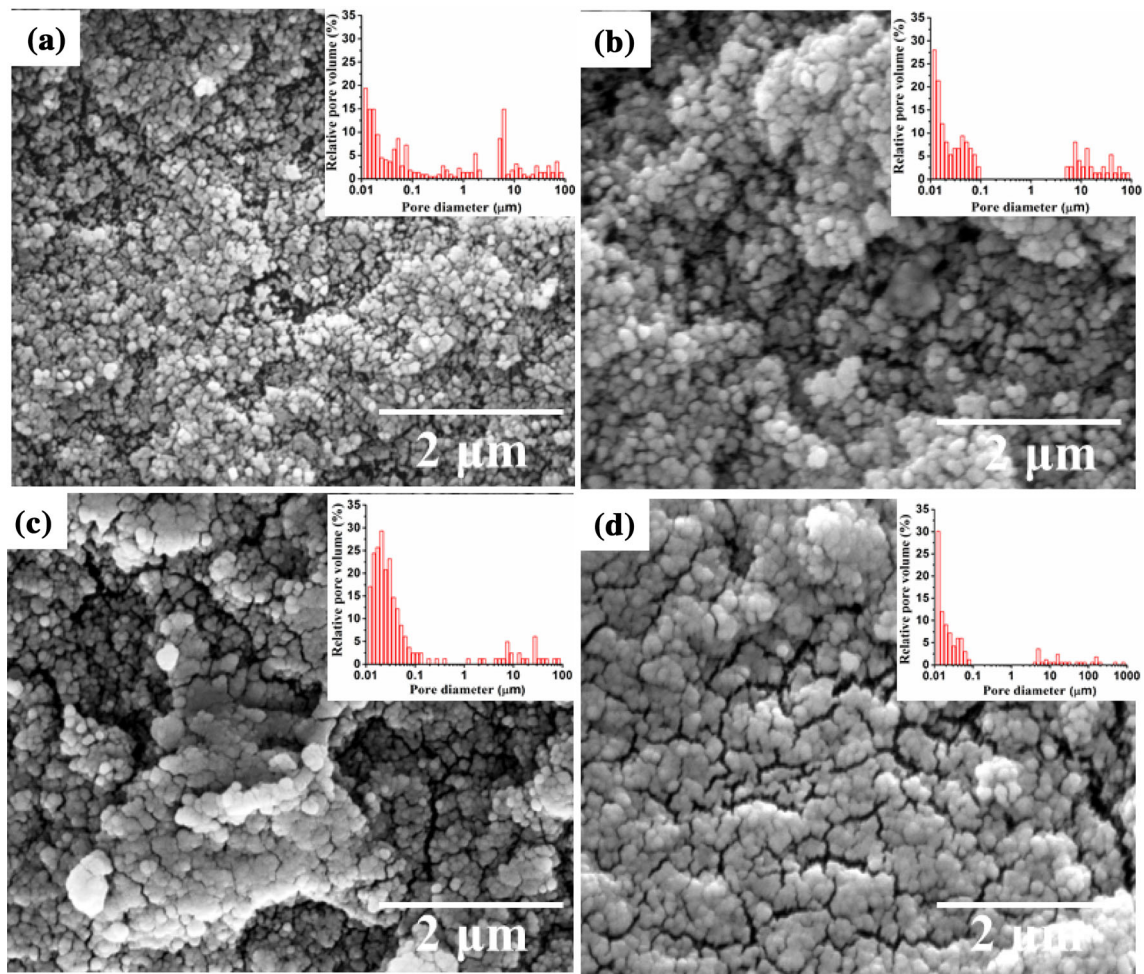


Figure 3 FESEM images of **a** HA-0, **b** HA-5, **c** HA-10, **d** HA-15, and pattern of pore size distribution of nanocomposites is in *inset* of their respective images.

nanocomposites where compactness increased with gelatin content. As we explained that the cross-linking was increased with gelatin concentration, this cross-linking offers more intermolecular association forming more number of junction points; as a result, the size of pores was reduced [33]. Thus, the nanocomposite (HA-15) with highest cross-linking appeared to be more compact with the smallest pore size.

Mechanical characterization of synthesized nanocomposites

The bone graft to be used in load-bearing application must have optimum strength and modulus to match with natural bone. To check the potentiality of synthesized nanocomposites in load-bearing application, the compressive strength and elastic modulus of

nanocomposites are evaluated and represented in Fig. 4. It is observed that the CMC-Gel-HA nanocomposites have strength and modulus in the range of 40–85 MPa and 0.4–1.2 GPa, respectively, analogous to human cancellous and cortical bone [66]. The mechanical strength of the CMC-Gel-HA nanocomposites was improved mainly by the strong interaction between CMC-HA, gelatin-HA and CMC-gelatin [42, 46]. All these interactions facilitated cross-linking among polymers and HA, which is responsible for the formation of mechanically strong bone graft. It also showed that the strength and modulus of HA-15 were drastically enhanced, almost tenfold of HA-0 composite. It depicts that the high intermolecular interactions driven the compact microstructure of nanocomposite has additional contribution in compressive strength and elastic modulus. The compressive stress–strain curves of

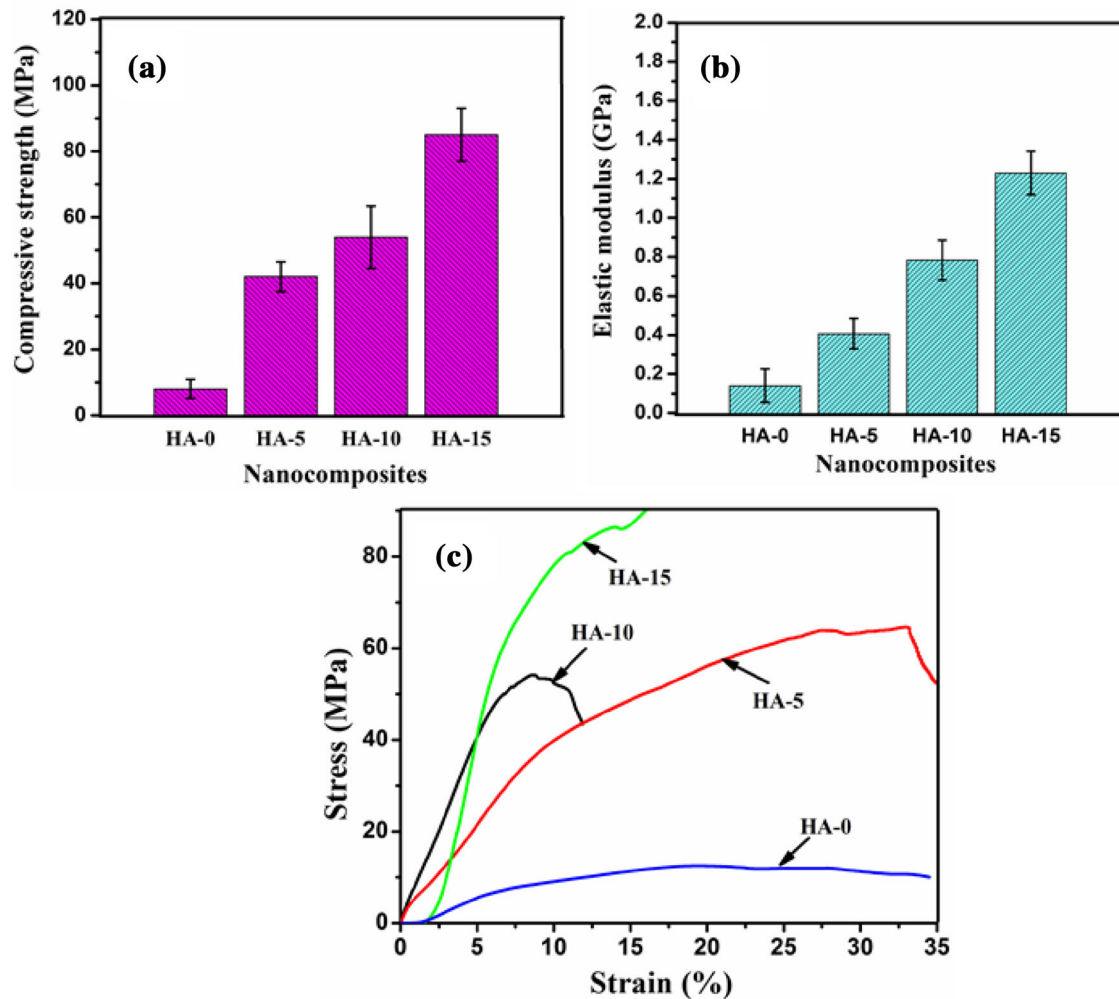


Figure 4 a Compressive strength and b elastic modulus of nanocomposites; c stress versus strain curves of nanocomposites.

nanocomposites are given in Fig. 4c. The variation in curve nature was observed, and HA-0 (without gelatin) deformed permanently after yield point due to comparatively weak interaction in CMC-HA and highly porous nature of nanocomposite. But, HA-5 composite showed viscoelastic deformation because the molecular interactions have been improved after incorporation of gelatin. The plastic region of stress-strain curves of HA-5 reflects the porous nature of composites, whereas compact HA-10 and HA-15 nanocomposites exhibited higher strength with lot of elastic strain energy indicating that the supportable load per unit surface area was maximum, with a low strain index. This observance manifested a rule of direct proportionality of stress-strain behavior of nanocomposites as a function of microstructure.

In vitro biocompatibility and proliferation study

The in vitro biocompatibility and proliferation of MG-63 cells were studied in the presence of nanocomposites extracts using MTT assay (Fig. 5a). In MTT assay, the absorbance due to metabolic activity of mitochondrial dehydrogenase of live cells was measured. The absorbance produced in HA-0, HA-5, HA-10 and HA-15 extracts showed the non-toxic nature of nanocomposites, and they are statistically significant to the control, which corresponds to each time period (1, 4 and 7 days). Furthermore, the cells proliferated to higher extent as the culture period is increased from 1 to 7 days in control as well as in samples extracts.

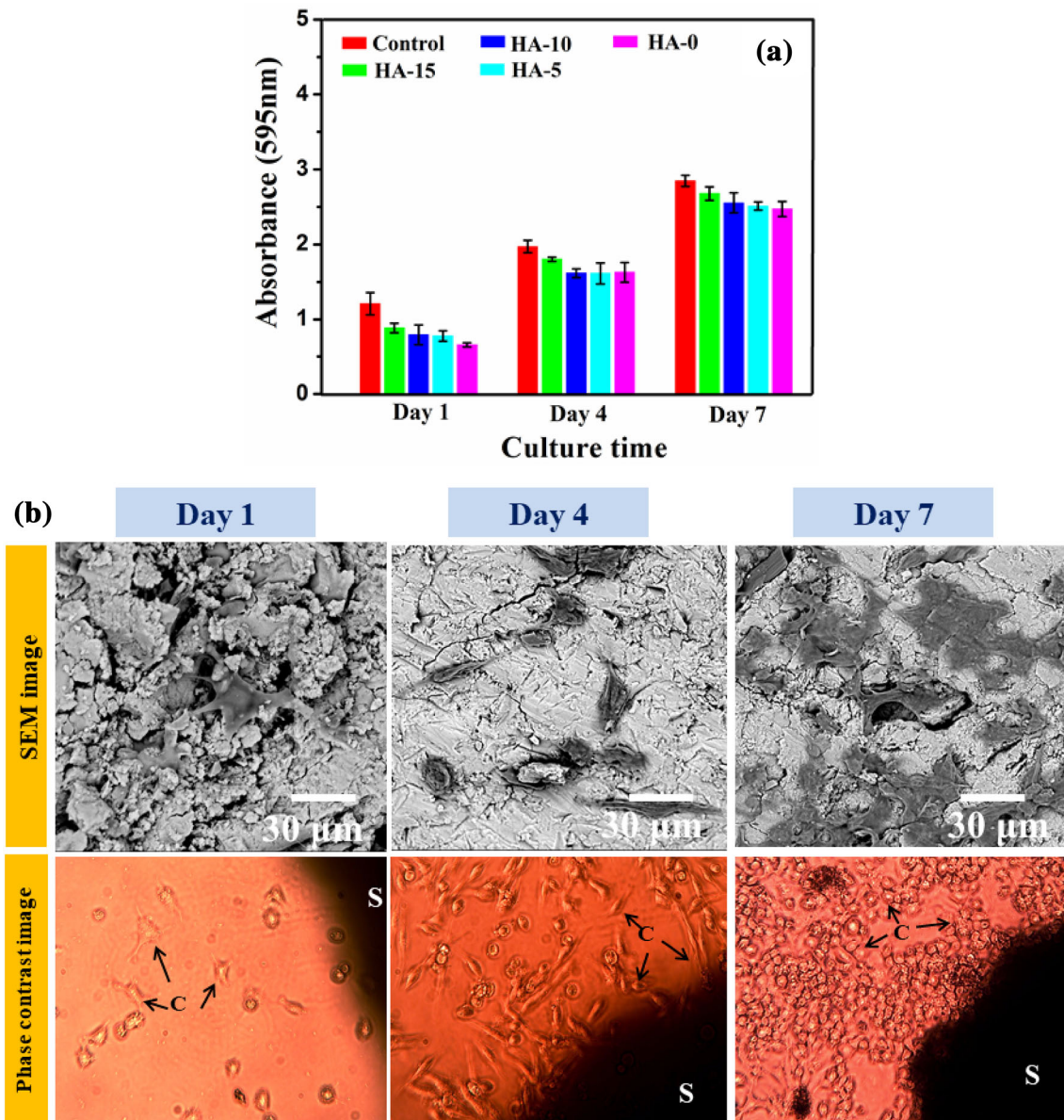


Figure 5 a MTT assay represented metabolic activity of MG-63 cells after cultured with nanocomposites extract (HA-0, HA-5, HA-10 and HA-15) for 1, 4 and 7 days (error bars represent the standard deviation, $n = 3$). b SEM micrograph and phase contrast

photographs of MG-63 cells cultured on HA-15 for 1, 4 and 7 days (scale bar in SEM = 30 μm, in phase contrast magnification = 10×, C denotes cell and S denotes sample).

Cellular behavior of MG-63 cells in close contact with CMC-Gel-HA nanocomposite was evaluated using SEM and phase contrast microscopy (Fig. 5b) after 1, 4 and 7 days of culture. In these images, MG-63 cells attached and spread well with cytoplasmic extension onto the surface of nanocomposite indicating that the environment of nanocomposite was well suited for cell growth and proliferation [67]. This

probably due to the large numbers of cell-binding peptides is available in CMC-Gel-HA nanocomposite. It promotes better cell-material interaction inducing more cellular activity [68, 69]. Thus, the cell density onto the samples was increased with incubation time from 1 to 7 days. The SEM images of cell seeded nanocomposites are consistent with corresponding phase contrast images of surrounding cells.

Evaluation of osteogenic differentiation

Alkaline phosphatase (ALP) is an early-stage osteogenic differentiation marker secreted by osteoblasts. For evaluating the osteogenic properties of load-bearing CMC-Gel-HA nanocomposite and the role of gelatin on the osteogenesis of nanocomposite, we have chosen the strongest HA-15 (CMC-Gel-HA) nanocomposite and HA-0 (CMC-

HA) nanocomposite for this study. We measured the ALP activity of MG-63 cells (Fig. 6a) cultured with nanocomposites [HA-0 and HA-15] for 7 and 14 days and compared with controls. Results showed that the ALP activity of cells at day 14 was remarkably increased in positive control and CMC-Gel-HA nanocomposite. But negative control and CMC-HA nanocomposite showed less production of alkaline phosphatase. The positive effect of

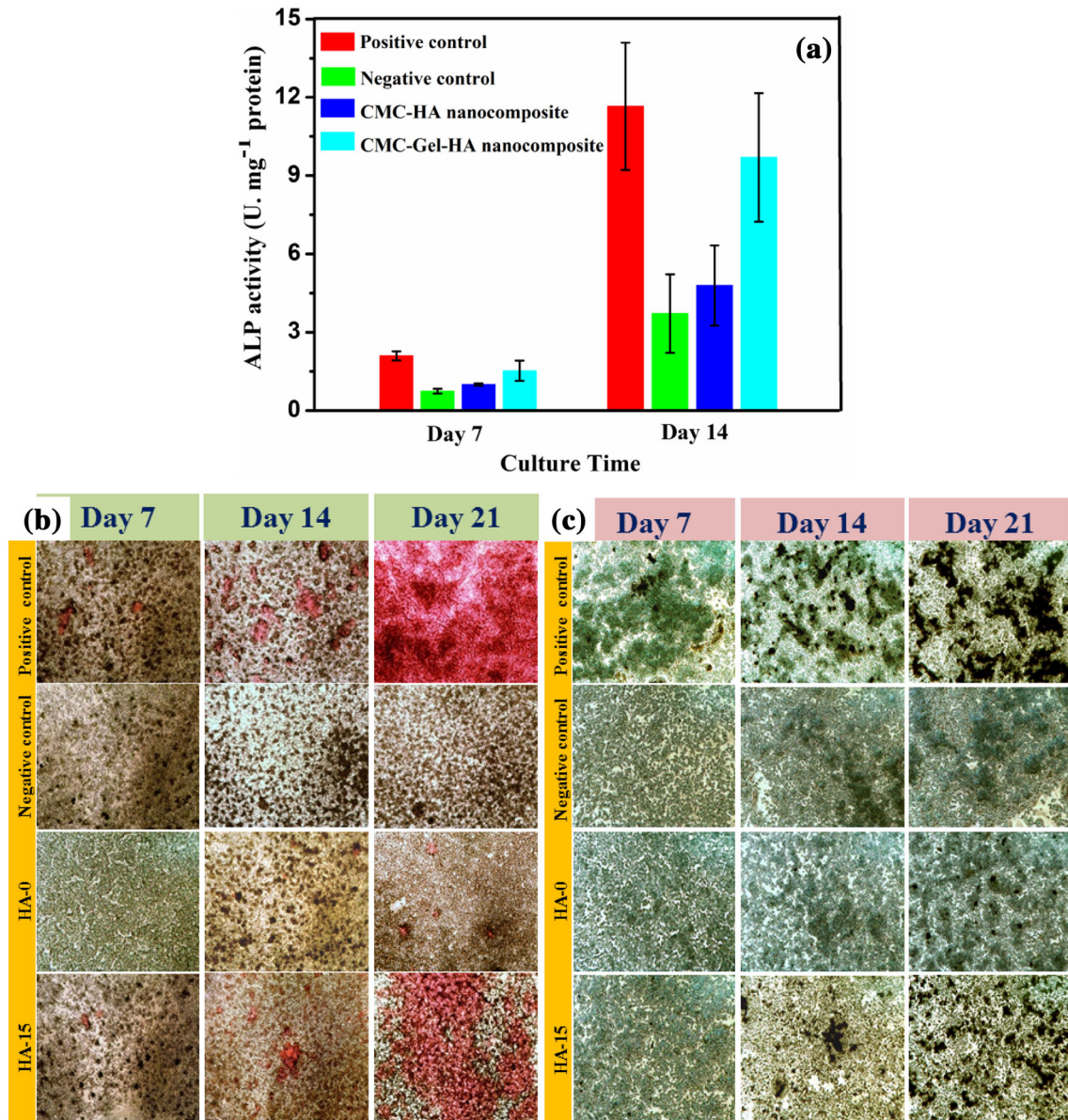


Figure 6 **a** Quantitative alkaline phosphatase (ALP) activity of MG-63 cells cultured with osteogenic media, basal media, CMC-HA nanocomposite (HA-0) and CMC-Gel-HA nanocomposite (HA-15) for 7 and 14 days (*error bars* represent the standard deviation, *n* = 3). Matrix mineralization of MG-63 cells after

in vitro culture with osteogenic media, basal media, CMC-HA nanocomposite (HA-0) and CMC-Gel-HA nanocomposite (HA-15) for 7, 14 and 21 days by, **b** alizarin red staining and **c** von Kossa staining.

CMC-Gel-HA nanocomposite on cells for high ALP activity was probably due to the presence of gelatin, an excellent contributor of osteogenesis [68, 69]. The mineralization of extracellular matrix (ECM) with calcium phosphate is a late-stage marker for osteogenic differentiation. Alizarin red staining and von Kossa staining are commonly used for detecting calcium phosphate present in the deposited mineral with red and deep brown coloration, respectively [23, 55]. Calcium phosphate depositions of MG-63 cells cultured with HA-0 and HA-15 for 7, 14 and 21 days are presented in Fig. 6b, c. At day 21, the remarkable calcium deposition was observed in HA-15 as well as in the positive control (Fig. 6b, c). Negative control does not show calcium deposition till the day 21, and CMC-HA nanocomposite shows very negligible mineralization on extracellular matrix. This result reliable with high ALP activity of cells in positive control and CMC-Gel-HA nanocomposite promotes more mineralization [70].

Biodegradation and bone apatite formation in SBF

Degradation of CMC-Gel-HA nanocomposite in SBF is shown in Fig. 7a. A continuous loss in weight is observed with time, and slight deflection is noticed in 28th day where weight of nanocomposite is not further reduced. In FTIR spectra of SBF-dipped CMC-Gel-HA nanocomposite (Fig. 7b), we found that the band at $3200\text{--}3160\text{ cm}^{-1}$ and 1384 cm^{-1} of synthesized nanocomposite (Fig. 1b) was disappeared in SBF-dipped samples indicating the breakage of cross-linking between polymers. Whether few small bands appeared at $1550\text{--}1300\text{ cm}^{-1}$ emphasized the breakage of cross-linking after incubation in SBF and gave individual polymeric bands. The surface micrographs of nanocomposite after immersion in SBF for 7, 14, 21 and 28 days are shown in Fig. 7c. Initially, the compact microstructure of nanocomposite started to break with the deposition of bone apatite on the surface of nanocomposite. With immersion time, the

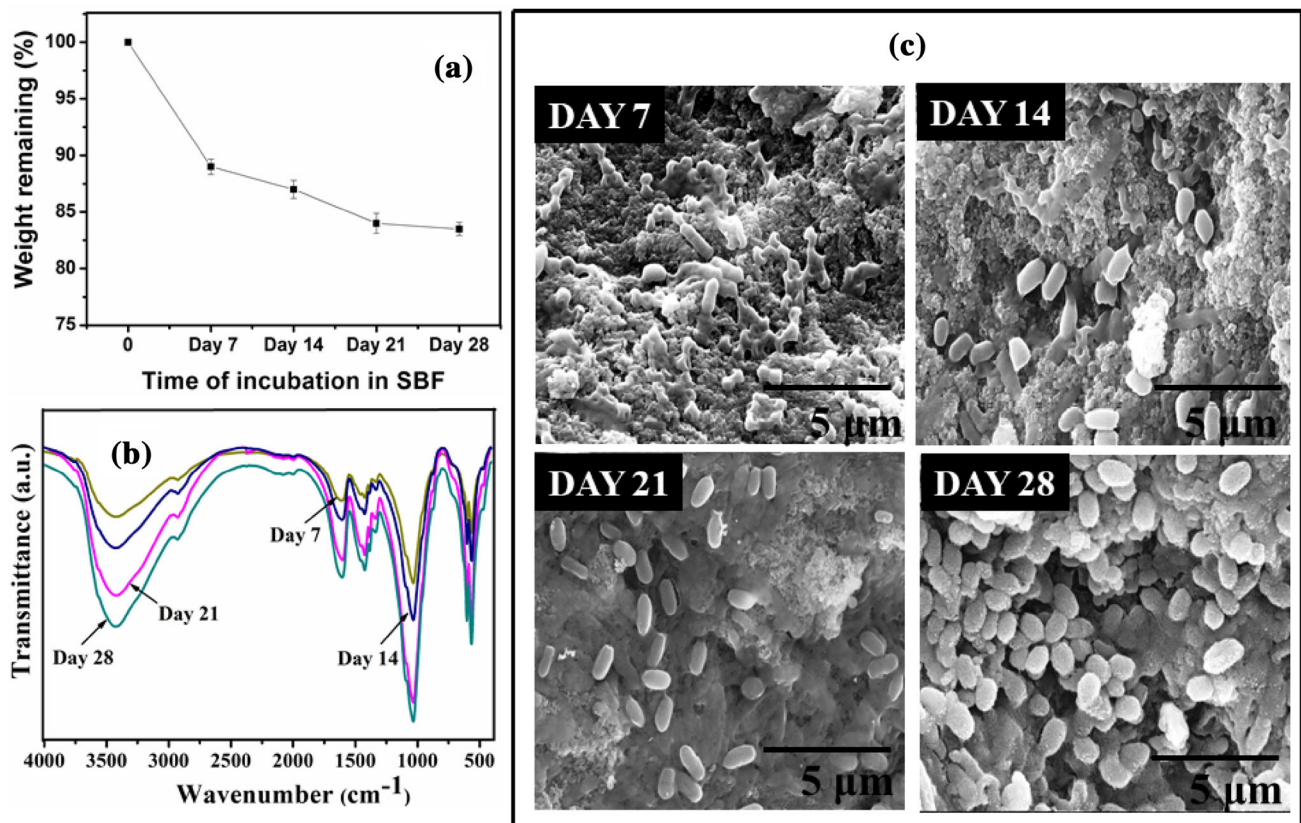


Figure 7 **a** Representative plot of weight remaining (%) versus time of CMC-Gel-HA nanocomposite immersed in SBF. **b** FTIR spectra of SBF-treated CMC-Gel-HA nanocomposite in different

incubation times. **c** Representative SEM images of SBF-treated CMC-Gel-HA nanocomposite in different incubation periods.

rate of bone apatite deposition increases and took oval-shaped agglomerate of size 1–1.5 μm (energy-dispersive spectrum (EDS) is given in Fig. S3). At day 28, the entire surface of nanocomposite was covered with these newly deposited apatites. Results ascertained the degradable nature and bone apatite deposition ability of synthesized nanocomposite in SBF. These newly deposited apatites may facilitate the bone-binding ability of CMC-Gel-HA nanocomposite in vivo.

Conclusions

In summary, this work developed a simple route for the synthesis of self-assembled CMC-Gel-HA nanocomposite as a load-bearing synthetic bone graft. The interfacial molecular interactions at the organic–inorganic interface assist the site specific nucleation and growth of HA nanoparticles in bridging position. The cross-linking between polymers via H-bonding and bridging HA molecules is the main driving force for the formation of a three-dimensional mechanically strong CMC-Gel-HA nanocomposite. The hybrid polymers matrix governs the morphology, function and self-assembled architecture of the nanocomposites. The mechanical compressive strength increases with the increase in gelatin content and exhibited systematic dependence with molecular interaction in the nanocomposites. This study sheds light on the possible use of templating agents for the synthesis of three-dimensional load bearing mechanically strong nanocomposites according to the desired properties and will open up the scope of using selective matrices for the synthesis of nanocomposites.

Acknowledgements

We acknowledge In House Project Support Group (iPSG) (OLP-0231), CSIR-National Metallurgical Laboratory, Jamshedpur, for funding. One of the authors (Chandrani Sarkar) would like to acknowledge University Grants Commission, India, for granting Senior Research Fellowship.

Compliance with ethical standards

Conflict of interest The authors declare that they have no conflict of interest.

Electronic supplementary material: The online version of this article (doi:[10.1007/s10853-017-1528-1](https://doi.org/10.1007/s10853-017-1528-1)) contains supplementary material, which is available to authorized users.

References

- [1] Giannoudis PV, Dinopoulos H, Tsiridis E (2005) Bone substitutes: an update Injry. *Int J Care Inj* 36:S20–S27
- [2] Brydone AS, Meek D, Maclaine S (2010) Bone grafting, orthopedic biomaterials, and the clinical need for bone engineering. *J Proc Inst Mech Eng H* 224:1329–1343
- [3] Barrere F, Mahmood TA, Groot KD, van Blitterswijk CA (2008) Advanced biomaterials for skeletal tissue regeneration: instructive and smart functions. *Mater Sci Eng, R* 59:38–71
- [4] Pina S, Oliveira JM, Reis RL (2015) Natural-based nanocomposites for bone tissue engineering and regenerative medicine: a review. *Adv Mater* 27:1143–1169
- [5] Armentano I, Dottori M, Fortunati E, Mattioli S, Kenny JM (2010) Biodegradable polymer matrix nanocomposites for tissue engineering: a review. *Polym Degrad Stab* 95:2126–2146
- [6] Yunos DM, Bretcanu O, Boccaccini AR (2008) Polymer-bioceramic composites for tissue engineering scaffolds. *J Mater Sci* 43:4433–4442. doi:[10.1007/s10853-008-2552-y](https://doi.org/10.1007/s10853-008-2552-y)
- [7] Kong L, Gao Y, Lu G, Gong Y, Zhao N, Zhang X (2006) A study on the bioactivity of chitosan/nano-hydroxyapatite composite scaffolds for bone tissue engineering. *Eur Polym J* 42:3171–3179
- [8] Chen J, Nan K, Yin S, Wang Y, Wu T, Zhang Q (2010) Characterization and biocompatibility of nanohybrid scaffold prepared via in situ crystallization of hydroxyapatite in chitosan matrix. *Coll Surf B* 81:640–647
- [9] Yang W, Both SK, Zuo Y, Birgani ZT, Habibovic P, Li Y, Jansen JA, Yang F (2015) Biological evaluation of porous aliphatic polyurethane/hydroxyapatite composite scaffolds for bone tissue engineering. *J Biomed Mater Res* 103:2251–2259
- [10] Sun F, Zhou H, Lee J (2011) Various preparation methods of highly porous hydroxyapatite/polymer nanoscale biocomposites for bone regeneration. *Acta Biomater* 7:3813–3828
- [11] Bleek K, Taubert A (2013) New developments in polymer-controlled, bioinspired calcium phosphate mineralization from aqueous solution. *Acta Biomater* 9:6283–6321
- [12] Wegst UGK, Bai H, Saiz E, Tomsia PA, Ritchie RO (2014) Bioinspired structural materials. *Nat Mater* 14:23–36
- [13] Minardi S, Corradetti B, Taraballi F, Sandri M, Eps JV, Cabrera F, Weiner BK, Tampieri A, Tasciotti E (2015)

- Evaluation of the osteoinductive potential of a bio-inspired scaffold mimicking the osteogenic niche, for bone augmentation. *Biomaterials* 62:128–137
- [14] Wells HC, Sizeland KH, Kirby N, Hawley A, Mudie S, Haverkamp RG (2015) Collagen fibril structure and strength in acellular dermal matrix materials of bovine, porcine, and human origin. *ACS Biomater Sci Eng* 1:1026–1038
- [15] Kane RJ, Weiss BHE, Meagher MJ, Liu Y, Gargac JA, Niebur GL, Wagner DR, Roeder RK (2015) Hydroxyapatite reinforced collagen scaffolds with improved architecture and mechanical properties. *Acta Biomater* 17:16–25
- [16] Kikuchi M, Suetsugu Y, Tanaka J, Ito S, Ichinose S, Shiniyama K, Hiraoka Y, Mandai Y, Nakatani S (1999) The biomimetic synthesis and biocompatibility of self-organized hydroxyapatite/collagen composites. *Bioceram* 12:393–396
- [17] Chang MC, Ikoma T, Kikuchi M, Tanaka J (2002) Crosslinkage of hydroxyapatite/collagen nanocomposite using glutaraldehyde. *J Mater Sci Mat Med* 13:993–997
- [18] Pek YS, Gao S, Arshad MSM, Leck KJ, Ying JY (2008) Porous collagen-apatite nanocomposite foams as bone regeneration scaffolds. *Biomaterials* 29:4300–4305
- [19] Chang MC, Ko CC, Douglas WH (2003) Preparation of hydroxyapatite-gelatin nanocomposite. *Biomaterials* 24:2853–2862
- [20] Azami M, Tavakol S, Samadikuchaksaraei A, Hashjin MS, Baheiraei N, Kamali M, Nourani MR (2012) A porous hydroxyapatite/gelatin nanocomposite scaffold for bone tissue repair: in vitro and in vivo evaluation. *J Biomater Sci* 23:2353–2368
- [21] Kim HW, Knowles JC, Kim HE (2005) Porous scaffolds of gelatin-hydroxyapatite nanocomposites obtained by biomimetic approach: characterization and antibiotic drug release. *J Biomed Mater Res B* 74:686–698
- [22] Kim HW, Kim HE, Salih V (2005) Stimulation of osteoblast responses to biomimetic nanocomposites of gelatin-hydroxyapatite for tissue engineering scaffolds. *Biomaterials* 26:5221–5230
- [23] Serra IR, Fradique R, Vallejo MCS, Correia TR, Miguel SP, Correia IJ (2015) Production and characterization of chitosan/gelatin/ β -TCP scaffolds for improved bone tissue regeneration. *Mater Sci Eng, C* 55:592–604
- [24] Sharma C, Dinda AK, Mishra NC (2012) Synthesis and characterization of glycine modified chitosan-gelatin-alginate composite scaffold for tissue engineering applications. *J Biomater Tiss Eng* 2:133–142
- [25] Luo Y, Lode A, Akkineni AR, Gelinsky M (2015) Concentrated gelatin/alginate composites for fabrication of pre-designed scaffolds with a favorable cell response by 3D plotting. *RSC Adv* 5:43480–43488
- [26] Balakrishnana B, Joshia N, Jayakrishnanb A, Banerjee R (2013) Self cross-linked oxidized alginate/gelatin hydrogel as injectable, adhesive biomimetic scaffolds for cartilage regeneration. *Acta biomaterial* 10:3650–3663
- [27] Gautam S, Chou CF, Dinda AK, Potdar PD, Mishra NC (2014) Fabrication and characterization of PCL/gelatin/chitosan ternary nanofibrous composite scaffold for tissue engineering applications. *J Mater Sci* 49:1076–1089. doi:10.1007/s10853-013-7785-8
- [28] Svensson A, Nicklasson E, Herrah T, Panilaitis B, Kaplan DL, Brittberg M, Gatenhol P (2005) Bacterial cellulose as a potential scaffold for tissue engineering of cartilage. *Biomaterials* 26:419–431
- [29] Brackmann C, Bodin A, Akason M, Gatenholm P, Enijder A (2010) Visualization of the cellulose biosynthesis and cell integration into cellulose scaffolds. *Biomacromol* 11:542–548
- [30] Hutchens SA, Benson RS, Evans BR, O'Neil HM, Rawn CJ (2006) Biomimetic synthesis of calcium deficient hydroxyapatite in a natural hydrogel. *Biomaterials* 27:4661–4670
- [31] Lii CY, Tomasik P, Zaleska H, Liaw SC, Lai VMF (2002) Carboxymethyl cellulose-gelatin complexes. *Carbohydr polym* 50:19–26
- [32] Taokaew S, Seetabhawang S, Siripong P, Phisalaphong M (2013) Biosynthesis and characterization of nanocellulose-gelatin films. *Materials* 6:782–794
- [33] Dash R, Foston M, Ragauskas AJ (2013) Improving the mechanical and thermal properties of gelatin hydrogels cross-linked by cellulose nanowhiskers. *Carbohydr Polym* 91:638–645
- [34] Rokhade AP, Agnihotri SA, Patil SA, Malliarjuna NN, Kulkarni PV, Aminabhavi TM (2006) Semi-interpenetrating polymer network microspheres of gelatin and sodium carboxymethyl cellulose for controlled release of ketorolac tromethamine. *Carbohydr Polym* 65:243–252
- [35] Wiwatwongwana F, Khunathon Y, Rangsi W, Promma N, Pattana S (2012) Identification of shear modulus of gelatin blended with carboxymethylcellulose scaffolds using curve fitting method from compressive test. *J Mater Sci Res* 1:106–113
- [36] Isikli C, Hasirci V, Hasirci N (2012) Development of porous chitosan-gelatin/hydroxyapatite composite scaffolds for hard tissue-engineering applications. *Tiss Eng Regen Med* 6:135–143
- [37] Sadeghi D, Nazarian H, Marouf N, Aghalu F, Nojehdehyan H, Dastjerdi EV (2013) Alkaline phosphatase activity of osteoblast cells on three-dimensional chitosan gelatin/hydroxyapatite composite scaffolds. *J Dent Sch* 30:203–209
- [38] Sharma C, Dinda AK, Potdar PD, Chou CF, Mishra NC (2016) Fabrication and characterization of novel nano-

- biocomposite scaffold of chitosan-gelatin-alginate-hydroxyapatite for bone tissue engineering. *Mater Sci Eng C* 64:416–427
- [39] Teng SH, Liang MH, Wang P, Luo Y (2016) Biomimetic composite microspheres of collagen/chitosan/nano-hydroxyapatite: in-situ synthesis and characterization. *Mater Sci Eng C* 58:610–613
- [40] Li J, Chen Y, Yin Y, Yao F, Yao K (2007) Modulation of nano-hydroxyapatite size via formation on chitosan-gelatin network film in situ. *Biomaterials* 28:781–790
- [41] Teng S, Shi J, Peng B, Chen L (2006) The effect of alginate addition on the structure and morphology of hydroxyapatite/gelatin nanocomposites. *Compos Sci Technol* 66:1532–1538
- [42] Garai S, Sinha A (2014) Biomimetic nanocomposites of carboxymethyl cellulose-hydroxyapatite: novel three dimensional load bearing bone grafts. *Coll Surf B* 115:182–190
- [43] George A, Ravindran S (2010) Protein templates in hard tissue engineering. *Nano today* 5:254–266
- [44] Cui FZ, Li Y, Ge J (2007) Self-assembly of mineralized collagen composites. *Mater Sci Eng R* 57:1–27
- [45] Farbod K, Nejadnik MR, Jansen JA, Leeuwenburgh SCG (2014) Interactions between inorganic and organic phases in bone tissue as a source of inspiration for design of novel nanocomposites. *Tiss Eng B* 20:173–188
- [46] Pei Y, Ye D, Zhao Q, Wang X, Zhang C, Huang W, Zhang N, Liu S, Zhang L (2015) Effective promoting wound healing with cellulose/gelatin sponges constructed directly from a cellulose solution. *J Mater Chem B* 3:7518–7528
- [47] Kim HL, Jung GY, Yoon JH, Han JS, Park YJ, Kim DG, Zhang M, Kim DJ (2015) Preparation and characterization of nano-sized hydroxyapatite/alginate/chitosan composite scaffolds for bone tissue engineering. *Mater Sci Eng C* 54:20–25
- [48] Koupaei N, Karkhaneh A, Joupari MD (2015) Preparation and characterization of (PCL-crosslinked-PEG)/hydroxyapatite as bone tissue engineering scaffolds. *J Biomed Mater Res* 103:3919–3929
- [49] Rodriguez IA, Saxena G, Hixon KR, Sell SA, Bowlin GL (2016) In vitro characterization of MG-63 osteoblast-like cells cultured on organic-inorganic lyophilized gelatin sponges for early bone healing. *J Biomed Mater Res* 104:2011–2019
- [50] Liyun J, Yubao L, Chendong X (2009) Preparation and biological properties of a novel composite scaffold of nano-hydroxyapatite/chitosan/Carboxymethyl cellulose for bone tissue engineering. *J Biomed Sci* 16:65–75
- [51] Liyun J, Yubao L, Li Z, Jianguo L (2008) Preparation and properties of a novel bone repair composite: nano-hydroxyapatite/chitosan/Carboxymethyl cellulose. *J Mater Sci Mater Med* 19:981–987
- [52] Zheng X, Zhou S, Xiao Y, Yu X, Feng B (2009) In situ preparation and characterization of a novel gelatin/poly(D, L-lactide)/hydroxyapatite nanocomposite. *J Biomed Mater Res B* 91:181–190
- [53] Rajzer I, Menaszek E, Bacakova L, Rom M, Blazewicz M (2010) In vitro and in vivo studies on biocompatibility of carbon fibers. *J Mater Sci Mater Med* 21:2611–2622
- [54] Chen J, Zhang X, Huang C, Cai H, Hu S, Wan Q, Pei X, Wang J (2017) Osteogenic activity and antibacterial effect of porous titanium modified with metal-organic framework films. *J Biomed Mater Res A* 105:834–846
- [55] Garai S, Sinha A (2016) Three dimensional biphasic calcium phosphate nanocomposites for loadbearing bioactive bone grafts. *Mater Sci Eng C* 59:375–383
- [56] Kokubo T, Kushitani H, Sakka S, Kitsugi T, Yamamuro T (1990) Solutions able to reproduce in vivo surface-structure changes in bioactive glass-ceramic A-W. *J Biomed Mater Res* 24:721–734
- [57] Li J, Zhu D, Yin J, Liu Y, Yao F, Yao K, Li J, Zhu D, Yin J, Liu Y, Yao F, Yao K (2010) Formation of nano-hydroxyapatite crystal in situ in chitosan-pectin polyelectrolyte complex network. *Mater Sci Eng C* 30:795–803
- [58] Li J, Dou Y, Yang J, Yin Y, Zhang H, Yao F, Wang H, Yao K (2009) Surface characterization and biocompatibility of micro- and nano-hydroxyapatite/chitosan-gelatin networks films. *Mater Sci Eng C* 29:1207–1215
- [59] Wang F, WenY Bai T (2016) The composite hydrogels of polyvinyl alcohol-gellan gum-Ca²⁺ with improved network structure and mechanical property. *Mater Sci Eng C* 69:268–275
- [60] Tu ZC, Huang T, Wang H, Sha XM, Shi Y, Huang XQ, Man ZZ, Li DJ (2015) Physico-chemical properties of gelatin from bighead carp (*Hypophthalmichthys nobilis*) scales by ultrasound-assisted extraction. *J Food Sci Technol* 52:2166–2174
- [61] Klug HP, Alexander LE (1974) X-ray diffraction procedures: for polycrystalline and amorphous materials, 2nd edn. Wiley, New York 4:960
- [62] Olszta MJ, Cheng X, Jee SS, Kumar R, Kim YY, Kaufman MJ, Douglas EP, Gower LB (2007) Bone structure and formation: a new perspective. *Mater Sci Eng R* 58:77–116
- [63] Busch S, Schwarz U, Kniep R (2001) Morphogenesis and structure of human teeth in relation to biomimetically grown fluorapatite-gelatin composites. *Chem Mater* 13:3260–3271
- [64] Murray MGS, Wang J, Ponton CB, Marquis PM (1995) An improvement in processing of hydroxyapatite ceramics. *J Mater Sci* 30:3061–3074. doi:10.1007/BF01209218
- [65] Sturm EV, Colfen H (2016) Mesocrystals: structural and morphogenetic aspects. *Chem Soc Rev* 45:5821–5833

- [66] Hench LL (1991) Bioceramics: from concept to clinic. *J Am Ceram Soc* 74:1487–1510
- [67] Anselme K (2000) Osteoblast adhesion on biomaterials. *Biomaterials* 21:667–681
- [68] Shi C, Yuan W, Khan M, Li Q, Feng Y, Yao F, Zhang W (2015) Hydrophilic PCU scaffolds prepared by grafting PEGMA and immobilizing gelatin to enhance cell adhesion and proliferation. *Mater Sci Eng C* 50:201–209
- [69] Kuo ZK, Lai PL, Toh EKW, Weng CH, Tseng HW, Chang PZ, Chen CC, Cheng CM (2016) Osteogenic differentiation of preosteoblasts on a hemostatic gelatin sponge. *Sci Rep* 6:32884–32896
- [70] Golub EE, Battaglia KB (2007) The role of alkaline phosphatase in mineralization. *Curr Opin Orthop* 18:444–448